ChemComm

COMMUNICATION

View Article Online
View Journal

Cite this: DOI: 10.1039/d4cc02128b

Received 3rd May 2024,
Accepted 17th June 2024

DOI: 10.1039/d4cc02128b

rsc.li/chemcomm

Multiscale characterizations of structural evolution in mesoporous CeO_2†

Tianyu Li and Efrain E. Rodriguez*

***In situ* ultra-small-angle and wide-angle X-ray scattering enables simultaneous tracking of the structural parameters of mesoporous CeO_2 from the atomic scale to the micron-size scale. This multiscale approach provides a path to better understand structure–property relationships in mesoporous polycrystalline materials under dynamic conditions such as high temperature cycling.**

Just as describing the structure of a protein necessitates experiments at multiple length scales, elucidating the structure of a functional material at different length scales, from the atomic to the macroscopic, is also required to understand its properties and performance. For example, the atomic structure, particle morphology and packing manner of electrode materials can all influence Li-ion battery performance.[1–3] In addition, the structures at different scales might also influence each other. For example, the size of the particles or grains, which are at the micron or nano scale, might determine the atomic structure of the material.[4,5]

Mesoporous materials illustrate this problem of multiple length scales since their performance is affected by the atomic structure constituting the pore walls, the specific pore topology, and finally the particle morphology. Mesoporous metal oxides are found in a wide variety of applications and fields such as heterogeneous catalysis and rechargeable batteries due to their high surface areas and favorable mass transport characteristics.[6,7] Nowadays, it is quite routine to characterize their structures at different length scales *via ex situ* methods. However, when those mesoporous materials are utilized in dynamic process (*e.g.*, charging/discharging in a battery or a catalytic cycle at elevated temperatures), their structures undoubtedly change, thereby altering the material's performance. In that case, *ex situ* experiments become less relevant to evaluate performance under real working conditions. To address such a shortcoming, researchers have developed multiple *in situ* structural characterization techniques.[8,9] Though it remains a challenge to perform simultaneous, multilength scale structural analyses *in situ*, such experiments should yield unprecedented insight into the complex interrelations among various features of functional material at different scales.

Due to their high importance in heterogenous catalysis, the materials we explored in the study are mesoporous ceria (CeO_2) in the SBA-15 and KIT-6 structures prepared *via* nanocasting.[10] The structure of mesoporous CeO_2 needs to be described at different scales. At the angstrom-scale, Ce and O atoms order *via* ionic bonds to form a crystalline phase with the fluorite-type structure. At the nanoscale, CeO_2 crystallites form nano-size grains that are further "stacked" into the ordered mesoporous structure. Finally, at the microscale, the mesoporous structures grow large enough to form near-micron-sized particles. These different scales can be characterized in a traditional, *ex situ* fashion. Indeed, we show such results for our mesoporous CeO_2 as independent verification such as powder X-ray diffraction, small angle X-ray scattering and transmission electron microscopy (the *ex situ* TEM are displayed in Fig. S1 and S2 (ESI†) to confirm the multi-scale structures of our CeO_2 samples).

In this communication the main experiment that goes beyond the *ex situ* methodology is the *in situ* scattering under heating conditions of our CeO_2 samples from atomic scale to micron scale. An ultra-small-angle X-ray scattering (USAXS) instrument with a wide angle scattering (WAXS) capability provides an extreme range in length scales,[11,12] ideal for simultaneous structural characterization of mesoporous materials. To this end, we utilized a synchrotron X-ray based USAXS instrument equipped with WAXS detectors on beamline 9-ID at the advanced photon source (Argonne National Laboratory). The *Q*-range of the combined USAXS/WAXS is 8×10^{-5} Å^{-1}–6 Å^{-1}, which gives characteristic scales ranging from 6×10^{-6} m to 1×10^{-10} m, *i.e.*, four orders of magnitude, in real space. This broad range is extensive enough to cover the nanostructures and microstructures of the studied materials.

We show one isotherm of the *in situ* USAXS and WAXS heating experiment in Fig. 1. We first demonstrate in the

---

Department of Chemistry and Biochemistry, University of Maryland, College Park, Maryland 20742-2115, USA. E-mail: efrain@umd.edu

† Electronic supplementary information (ESI) available. See DOI: **https://doi.org/10.1039/d4cc02128b**

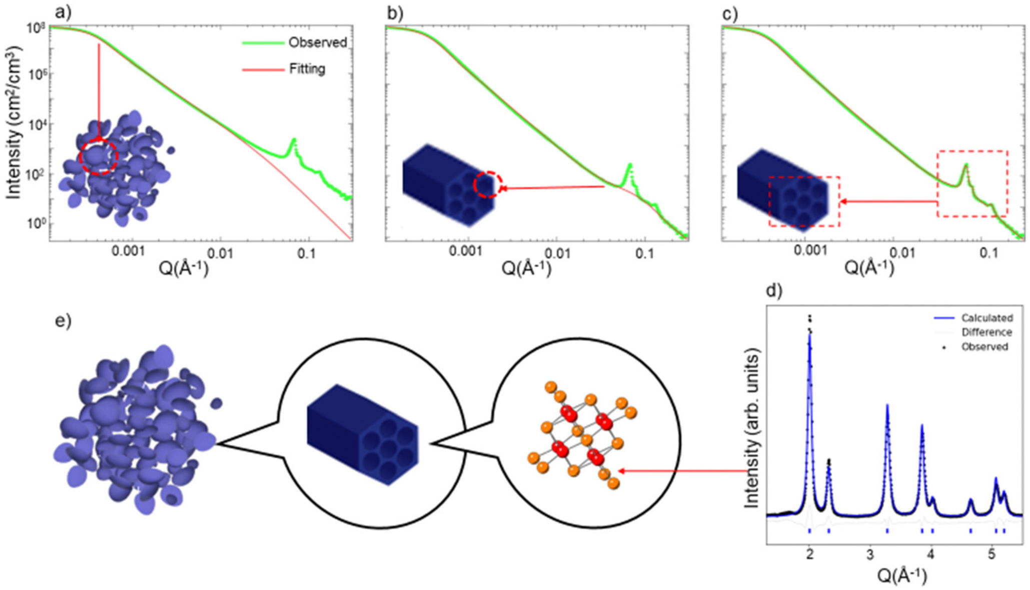

Fig. 1 USAXS data fitted considering (a) Only particle size, (b) particle size and mesopore size, (c) particle size, mesopore size and ordered pore structures. (d) WAXS/XRD pattern with Rietveld refinement. (e) Illustration of the structure of mesoporous CeO_2 at different scales. Data are collected on SBA-15 templated mesoporous CeO_2 at 50 °C. USAXS data is plotted at log scale for both axes.

SBA-15 templated mesoporous CeO_2 how the different regions of the USAXS/WAXS data correlate to the real space structures. At the extremely low Q region of the USAXS data ($Q < 0.001$ Å^{-1}), the curve reflects the micro-scale to meso-scale (>100 nm) structure information of the mesoporous material particles. By fitting a simple unified model (Fig. 1a) (composed of a Guinier part and a power law tail),[13,14] the radius of gyration (R_g) of the particle can be estimated and should be comparable to the particle size.

At the high-Q region ($Q > 0.01$ Å^{-1}), two features are noted. First, the uptrend of the curve at high Q region does not match fitted curve when only particle structure is considered in the fitting model (Fig. 1a). By adding a second unified model with much smaller R_g (∼30 Å), the curve at low-Q region can be well fit, as is displayed in Fig. 1b. We attribute this uptrend in the curve to the scattering due to each individual mesopore, *i.e.*, the pore's form factor. The pore size of the mesoporous CeO_2 is measured from TEM image (Fig. S1, ESI†), which is around 30–40 Å, comparable to the fitted R_g value obtained from the high-Q region. The second feature at the high-Q region is the appearance of several sharp peaks, which is a result of the diffraction from the ordered mesopore structures. These diffraction peaks contain information such as manner of the ordering (symmetries and distance between lattice planes) and degree of the ordering. The diffraction peaks shown in USAXS data correspond to the hexagonal pores of SBA-15 CeO_2 and can be indexed to the *p6mm* plane group, while the mesopores of KIT-6 CeO_2 are described by the *Ia3d* space group.[10] The diffraction peaks in USAXS data can be fit with certain peak shapes individually (Fig. 1c), and peak position and half width information can be extracted simultaneously.

Outside of the USAXS data, the WAXS data ($Q > 1$ Å^{-1}) contains the information about atomic arrangement in the materials. By performing Rietveld refinement analysis[15] with the diffraction patterns (Fig. 1d), we can track the change of the crystal structure, crystallinity (grain size) and lattice expansion.

For the *in situ* structure characterization upon heating, the USAXS/WAXS patterns were continuously taken at different temperature steps. Throughout the experiment, our mesoporous CeO_2 powder samples were heated in air. In the first experiment, we heated the sample up to 1000 °C and cooled it down at the same rate down to 100 °C. The collected USAXS/WAXS patterns at different temperatures were fitted with the previously mentioned methods to extract important structural parameters at different length scales.

Fig. 2a and b display the *in situ* USAXS and WAXS patterns of SBA-15 templated CeO_2 powders upon heating to 1000 °C. A two-dimensional (2D) representation or contour plot of the data is provided in Fig. S4 and S5 (ESI†). Visually, the diffraction peaks in the USAXS start to deform at 800 °C, indicating the collapse of the ordered pore structure. The bump (indicated with black arrows in Fig. 2a), which we attribute to the scattering from individual pores, shifts to the lower Q region at 800 °C as well. This shift to lower Q implies that the size of mesopores becomes larger. In the WAXS (Fig. 2b), the diffraction peaks start to become sharper at 800 °C, suggesting an increase of crystalline grain size. The red curves in Fig. 2c shows change of the R_g of pores (from USAXS data fitting) and crystalline grain size (from WAXS Rietveld refinement) upon heating/cooling. Both values start to show an uptrend at around 700 °C and this uptrend becomes more obvious at 800 °C.

The *in situ* USAXS/WAXS experiments indicate that the collapse of the ordered pore structure, enlargement of the pore size and the recrystallization of the crystalline grains correlates to each other since they happen at nearly the same pace. We infer that the heating triggered the recrystallization process of the crystalline grains, which causes the fusion of the initial

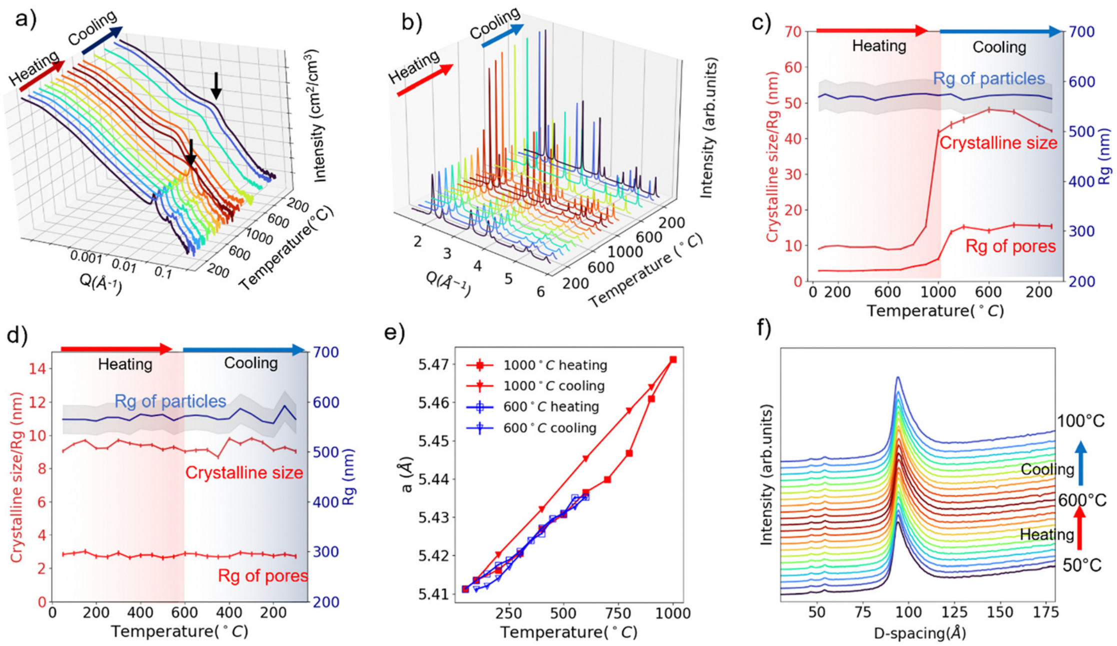

Fig. 2 *In situ* USAXS patterns (a) and WAXS patterns(b) under heating/cooling to/from 1000 °C. Extracted grain size, R_g of pores and R_g of particles under heating/cooling to/from 1000 °C (c) and under heating/cooling to/from 600 °C (d). Lattice expansion under heating/cooling to/from 1000 °C and under heating/cooling to/from 600 °C (e). (100) Diffraction peak from the ordered mesopores under heating/cooling to/from 600 °C (f). Data are collected for SBA-15 templated mesoporous CeO_2. USAXS data (a) is plotted at log scale for Q and intensity.

grains into larger grains. Crystalline CeO_2 is known to have a relatively high melting point (2400 °C). However, in the mesoporous CeO_2, CeO_2 exists in a nanocrystalline form (~10 nm), which will lead to a significantly enhanced surface tension and thus a lower melting point.[16] Thus, the fusion of CeO_2 nano grains happens at a much lower temperature than the actual melting point. And this fusion process between the "building blocks" of ordered mesopore structure leads to both the collapse of the ordered structure and the appearance of larger pores. The *in situ* TEM heating experiment up to 1000 °C (Fig. S6, ESI†) shows the evidence of fusion of crystalline grains and appearance of larger pores due to the fusion, which agrees well with the USAXS/WAXS data. Interestingly, the USAXS in the low-Q region does not show any significant changes upon heating to 1000 °C. The fitted R_g value for particles remains nearly unchanged during the whole experiment, as is indicated by the blue curve in Fig. 2c. Such an observation suggests the recrystallization/fusion only happens between crystalline grains in the porous structure but not in the packed mesoporous particles up to 1000 °C. Upon cooling, the R_g of pores and crystalline grain size maintains its value and does not recover back to the original state, which is intuitively reasonable as the recrystallization is not a reversible process.

The 1000 °C *in situ* heating experiment shows that the SBA-15 templated mesoporous CeO_2 seems to be durable upon heating up to 600 °C. Thus, we performed another *in situ* characterization on new powder samples with a 600 °C heating and cooling cycle. USAXS and WAXS data are displayed in Fig. S7 and S8 (ESI†), and the fitted size parameters are displayed in Fig. 2d. No significant changes were observed in both scattering patterns and fitted parameters, suggesting a good thermal and cycling stability of the structure at all scales up to 600 °C.

The lattice parameters can also be extracted from Rietveld refinement with the WAXS pattern. The lattice parameter changes upon 600 °C heating/cooling cycle and 1000 °C heating/cooling cycle are plotted in Fig. 2e. The thermal expansion of the lattice is observed. However, it is obvious the thermal expansion for 1000 °C cooling is larger than 1000 °C heating or 600 °C heating/cooling ($\alpha = 1.172 \times 10^{-5}$ °C^{-1} *vs.* 0.848×10^{-5} °C^{-1}). As mentioned previously, during the 1000 °C cooling step, the ordered mesoporous structure is lost and crystalline size enlarged. We thus conclude that the mesoporous structure alleviates the thermal expansion of CeO_2, which might be a result of strain from the porous structure or surface tension from the nano-sized grains.[17,18]

Theoretically, the expansion of the pore structure or particles can also be tracked by monitoring the diffraction peak shifts in the USAXS patterns. Fig. 2f displays the tracking of (100) diffraction peak (USAXS data) of the hexagonal pore structure upon 600 °C heating/cooling. A shift from 93.9 Å to 94.4 Å (USAXS resolution 0.1 Å^{-1}) is observed upon heating to 600 °C from 50 °C, corresponding to a thermal expansion coefficient of 0.97×10^{-5} °C^{-1}, which is comparable to the value (0.848×10^{-5} °C^{-1}) extracted from atomic lattice parameter change. Cooling leads to the shift back to smaller *d*-spacing, indicating the pore structure thermal expansion is reversible up to 600 °C. However, we are not able to determine whether the pore structure thermal expansion or atomic lattice thermal expansion is more significant (0.97×10^{-5} °C^{-1} *vs.*

0.848×10^{-5} °C^{-1}) due to the resolution limit of the USAXS experiment at the time.

Similar *in situ* heating USAXS/WAXS experiments are also performed on KIT-6 templated mesoporous CeO_2. The USAXS/WAXS patterns and fitted parameters for 1000 °C heating/cooling are 600 °C heating/cooling are presented on Fig. S11 and S12 (ESI†), respectively. Though both R_g of pores and crystalline grain size start to become larger at 700 °C (Fig. S11c, ESI†), same as SBA-15 templated mesoporous CeO_2, the diminishment of diffraction peak from ordered structure is only visible beyond 900 °C (800 °C for SBA-15 templated mesoporous CeO_2) (Fig. S11a, ESI†), suggesting the *Ia*3*d* ordered pore structure is more durable towards heating than *p*6*mm* ordered pore structure. The recrystallization/fusion similarly only happens between crystalline grains in the porous structure but not packed mesoporous particles up to 1000 °C as both high-Q region of USAXS data and the fitted R_g for particles do not show significant change (Fig. S11a and c, ESI†).

The enlargement of R_g for the pore upon heating seems to be more significant than the SBA-15 templated CeO_2, as indicated by the shift of the bump and fitted R_g value change (from 3 to 25 nm *vs.* from 3 to 10 nm, shown on Fig. S11c, ESI† and Fig. 2c). For 600 °C heating/cooling cycles, KIT-6 templated mesoporous CeO_2 shows similar good thermal and cycling stability (Fig. S12, ESI†). The lattice parameter changes upon 600 °C heating/cooling cycle and 1000 °C heating/cooling cycle are also extracted and plotted in Fig. S13 (ESI†). The smaller lattice thermal expansion on ordered porous structure is again observed ($\alpha = 1.197 \times 10^{-5}$ °C^{-1} for 1000 °C cooling *vs.* 0.847×10^{-5} °C^{-1} for others). Fig. S14 (ESI†) displays the tracking of *d*-spacing of (211) diffraction peak (USAXS data) of the cubic pore structure upon 600 °C heating/cooling. A shift from 92.3 Å to 93.0 Å is observed upon heating to 600 °C from 50 °C, corresponding to a thermal expansion coefficient of 1.37×10^{-5} °C^{-1}. Again, we are not able to use this value to make any conclusive comparisons due to the resolution limit.

In summary, we demonstrate how *in situ* structural characterization of mesoporous CeO_2 powder samples at different scales can be simultaneously obtained *via* synchrotron X-ray based USAXS/WAXS. Our study introduces an effective approach to monitor the evolution of particle size, pore structures, pore size, grain size and atomic structure of the mesoporous materials under dynamic conditions. Furthermore, we highlight that the structures of materials at different scales can influence each other, a factor that has not received sufficient attention in previous studies on mesoporous materials. Future research should focus more on understanding the interplay between structures at different scales and exploring its impact on material performance. Future experiments could expand beyond heating/cooling cycles to include gas flowing for catalytic reactions and charging/discharging for batteries. The multiscale *in situ* structural characterization will provide deep insights of the correlation between structural features at different scales and their synergistic impact on materials performance. Exploring the impact of rare metal cluster/single atom loading on the structural behaviors of mesoporous oxides will be also of great interest, as the loading can significantly influence the surface energy and strain of mesoporous materials, which, in turn, can affect their structural evolution under dynamic conditions.

This work is supported by the Department of Defense (grant HDTRA1-19-1-0001) and Department of Commerce (grant 70NANB20H139). Use of the Advanced Photon Source at Argonne National Laboratory was supported by the U.S. Department of Energy, Office of Science, Office of Basic Energy Sciences, under Contract No. DE-AC02-06CH11357. We thank Dr Jan Ilavsky, and Dr Ivan Kuzmenko at beamline 9ID, for their help with USAXS data collection and sample preparation.

Data availability

The data supporting this article have been included as part of the ESI.† *In situ* scattering data sets for this article are available at Open Science Framework at 10.17605/OSF.IO/2K4XA.

Conflicts of interest

The authors declare no competing financial interest.

References

1 A. Van Der Ven, J. Bhattacharya and A. A. Belak, *Acc. Chem. Res.*, 2013, **46**, 1216–1225.
2 D.-W. Chung, P. R. Shearing, N. P. Brandon, S. J. Harris and R. E. García, *J. Electrochem. Soc.*, 2014, **161**, A422–A430.
3 M. K. Devaraju and I. Honma, *Adv. Energy Mater.*, 2012, **2**, 284–297.
4 M. Yashima, T. Hoshina, D. Ishimura, S. Kobayashi, W. Nakamura, T. Tsurumi and S. Wada, *J. Appl. Phys.*, 2005, **98**, 014313.
5 J. Chen, L. Fan, Y. Ren, Z. Pan, J. Deng, R. Yu and X. Xing, *Phys. Rev. Lett.*, 2013, **110**, 115901.
6 U. Ciesla and F. Schüth, *Microporous Mesoporous Mater.*, 1999, **27**, 131–149.
7 Y. Ren, Z. Ma and P. G. Bruce, *Chem. Soc. Rev.*, 2012, **41**, 4909–4927.
8 L. Liu, *Trends Chem.*, 2021, **3**, 898–901.
9 Q. Meyer, Y. Zeng and C. Zhao, *Adv. Mater.*, 2019, **31**, 1901900.
10 S. C. Laha and R. Ryoo, *Chem. Commun.*, 2003, 2138–2139.
11 J. Ilavsky, F. Zhang, R. N. Andrews, I. Kuzmenko, P. R. Jemian, L. E. Levine and A. J. Allen, *J. Appl. Crystallogr.*, 2018, **51**, 867–882.
12 J. Ilavsky, F. Zhang, A. J. Allen, L. E. Levine, P. R. Jemian and G. G. Long, *Metall. Mater. Trans. A*, 2013, **44**, 68–76.
13 G. Beaucage, *J. Appl. Crystallogr.*, 1995, **28**, 717–728.
14 J. Ilavsky and P. R. Jemian, *J. Appl. Crystallogr.*, 2009, **42**, 347–353.
15 R. W. Cheary and A. Coelho, *J. Appl. Crystallogr.*, 1992, **2**, 109–121.
16 D. A. Porter, K. E. Easterling and K. E. Easterling, *Phase Transformations in Metals and Alloys (Revised Reprint)*, CRC Press, 2009.
17 Q. Li, H. Zhu, L. Hu, J. Chen and X. Xing, *Acc. Chem. Res.*, 2019, **52**, 2694–2702.
18 S. Elomari, M. D. Skibo, A. Sundarrajan and H. Richards, *Compos. Sci. Technol.*, 1998, **58**, 369–376.